

# Microstructure and Properties of Ni-SiC Nanocomposites Fabricated by Ultrasonic-Assisted Electrodeposition

Chunyang Ma<sup>1</sup>, Danqiong Zhao<sup>1</sup>, Hanzhao Xia<sup>2</sup>, Fafeng Xia<sup>1</sup>, Zhipeng Ma<sup>1,\*</sup>, Tom Williams<sup>3</sup>

<sup>1</sup> College of Mechanical Science and Engineering, Northeast Petroleum University, Daqing 163318, China;

<sup>2</sup> Shandong Tai'an No. 1 Senior High School, Tai'an 271000, China

<sup>3</sup> Department of Mechanical & Materials Engineering, University of Cincinnati, Cincinnati, OH 45221, USA

\*E-mail: [chunyangandma1@163.com](mailto:chunyangandma1@163.com)

Received: 9 January 2020 / Accepted: 17 February 2020 / Published: 10 April 2020

---

In this research, Ni-SiC nanocomposites (NCs) were effectively prepared by using ultrasonic-assisted electrodeposition (UAED). Effect of ultrasonic power on surface morphology, microstructure, phase composition and other NC properties was studied by scanning electron and atomic force microscopies, X-ray diffractometry as well as by microhardness, abrasion and electrochemical tests. The results indicated that Ni-SiC-300 NC, deposited at 300 W, showed smooth and fine-grained surface morphology with SiC nanoparticles (NPs) evenly distributed on the NC surface. As ultrasonic power was gradually changed from 100 to 400 W, XRD peaks corresponding to Ni matrix first broadened but then narrowed. Thus, only certain ultrasonic power (equal to 300 W in this case) was beneficial for the optimum Ni grain refinement of the resulting Ni-SiC NCs. Ni-SiC-300 NCs also demonstrated the highest microhardness (equal to 906.7 Hv), the best wear rate (equal to 17.8 mg/min) and the best corrosion resistance judging by its lowest corrosion current density (equal to 0.032  $\mu\text{A}/\text{mm}^2$ ).

---

**Keywords:** Ni-SiC NCs; Surface morphology; Property; Ultrasonic-assisted electrodeposition

## 1. INTRODUCTION

Ni-based composites are currently used in industries related to petroleum and other chemical fields because of their excellent chemical, mechanical and physical properties [1-5]. However, to improve performance of these composites in severe environments, they are often modified with ceramic particles (such as TiN, AlN, and SiC). In fact, Ni-SiC [6], Ni-AlN [7, 8], Ni-Mo-Al<sub>2</sub>O<sub>3</sub> [9] and Ni-TiN [10] composites were successfully obtained. Incorporation of ceramic particles into metallic Ni changes microstructure, grain size and crystal orientation of the matrix, which typically enhances overall composite properties.

To fabricate Ni-based composites containing ceramic fillers (NBCCs), synthesis techniques such as electrodeposition, electroless plating, casting as well as thermal spraying are typically used [11-13]. Among them, electrodeposition is the easiest as well as the most effective and appropriate technique for NBCC fabrication [14-16]. Several research groups implemented electrodeposition for composite preparation. Alizadeh *et al.* [17] studied Ni-Mo/Al<sub>2</sub>O<sub>3</sub> nanocomposites (NCs) synthesized using electrodeposition and found homogeneously distributed Al<sub>2</sub>O<sub>3</sub> particles in the metallic Ni. Dehghani *et al.* [18] analyzed corrosion resistance and microstructure of electrodeposited Ni-Al<sub>2</sub>O<sub>3</sub>-SiC NCs and reported substantially enhanced corrosion resistance of these NCs especially in comparison to unmodified Ni.

Ultrasonic agitation is a typical technique used during electrodeposition to disperse NPs in the plating liquid and to minimize their agglomeration [19]. In addition, performance of NBCCs obtained using ultrasonic-assisted electrodeposition (UAED) mainly relies on plating parameters, such as electrolyte temperature, ultrasonic power, current density, particle concentration and plating bath composition [20]. Among them, ultrasonic power significantly affects microstructure, phase structure, surface morphology and other properties of the resulting composites [21].

SiC, because of its high strength and hardness, is very often used for composite reinforcement, even those already possessing outstanding physical and chemical properties. Thus, in this work, we used UAED to incorporate SiC nanoparticles (NPs) into Ni to obtain SiC-reinforced NCs. We thoroughly analyzed how ultrasonic power affected microstructure, phase composition, surface morphology and other properties of the resulting NCs.

## 2. EXPERIMENTAL PROCEDURE

30×15×4 mm<sup>3</sup> A3 steel plate was used as a cathode. Prior to plating, the steel plates were washed to remove oil residue, rinsed with acetone, and then activated with nitric acid. Composition of the plating solution (which was used as an electrolyte) is shown in Table 1.

**Table 1.** Chemical composition of the electrolyte used during Ni–SiC NC preparation.

Sample	Ni-SiC nanocomposite (Ni-SiC-100)	Ni-SiC nanocomposite (Ni-SiC-200)	Ni-SiC nanocomposite (Ni-SiC-300)	Ni-SiC nanocomposite (Ni-SiC-400)
NiSO <sub>4</sub> (g/l)	280	280	280	280
NiCl <sub>2</sub> (g/l)	28	28	28	28
H <sub>3</sub> BO <sub>3</sub> (g/l)	25	25	25	25
SiC nanoparticles (g/l)	7	7	7	7
Cetyltrimethyl ammonium bromide (mg/l)	70	70	70	70
Current density (A/dm <sup>2</sup> )	4	4	4	4
Duty cycle (%)	30	30	30	30
Ultrasonic power (W)	100	200	300	400
pH	4.6	4.6	4.6	4.6
Plating time (min)	30	30	30	30

SiC NPs, ~40 nm in diameter, were added to the plating solution, which was then ultrasonically treated using XL-500 agitator. Experimental steps of Ni-SiC NCs fabrication procedure are schematically shown in Fig. 1.  $60 \times 30 \times 8 \text{ mm}^3$  Ni plate acted as an anode. SMD-200 power supply was employed to produce different current densities. Electrolyte temperature was maintained at  $46^\circ\text{C}$ . Ultrasonic powers used to synthesize different composites were 100, 200, 300, and 400 W, respectively. The depositing time was 30 min, and the solution pH was 4.6.

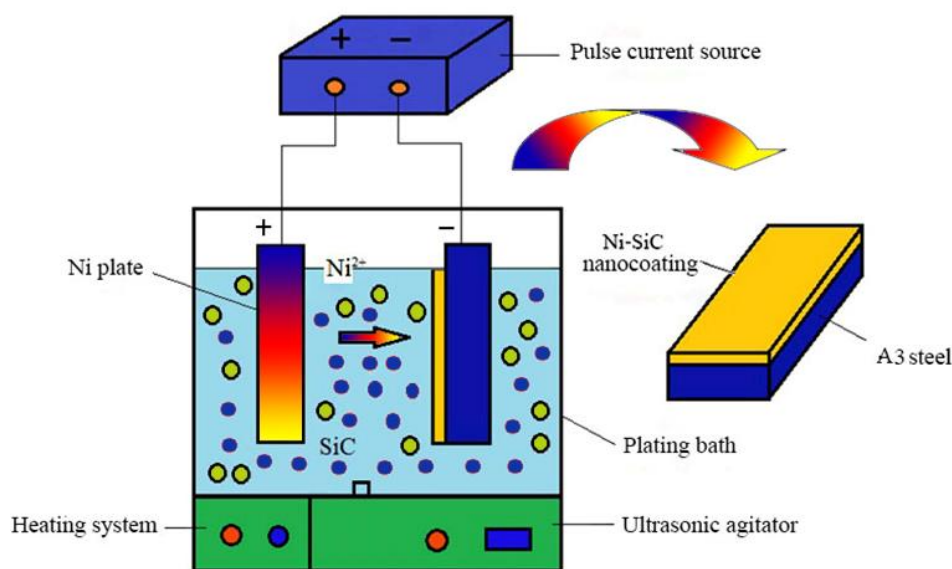


**Figure 1.** Schematic showing fabrication steps of Ni-SiC NCs.

Surface morphologies and chemical composition of all samples were studied using scanning electron microscopy (SEM, performed using S-4800 instrument) coupled with the energy dispersive spectroscopy (EDS, INCA) and atomic force microscopy (AFM, NT-MDT). X-ray diffraction (XRD) performed using D/Max-2400 instrument was conducted to phase composition determination.

Microhardness was tested by a VTD511 instrument using 50 gf load applied for 10 s. Friction and wear analyses (results of which are shown in Fig. 2) were conducted at dry sliding conditions and at ambient temperature using MRH-6 instrument containing a hardened steel hoop (GC15, with a sliding length equal to 150 m) applied to the NC surfaces at 0.1 m/s speed and 5 N load. Wear surfaces were studied by laser scanning confocal microscopy (LSCM, OLS4100) and SEM. All samples were weighed before and after the wear and friction tests. Wear rates ( $V$ ) were calculated as follows:

$$V = \frac{M_1 - M_2}{L} \quad (1),$$

where  $M_1$  and  $M_2$  are specimen weights before and after the wear tests, respectively, and  $L$  is the sliding length (equal to 150 m).

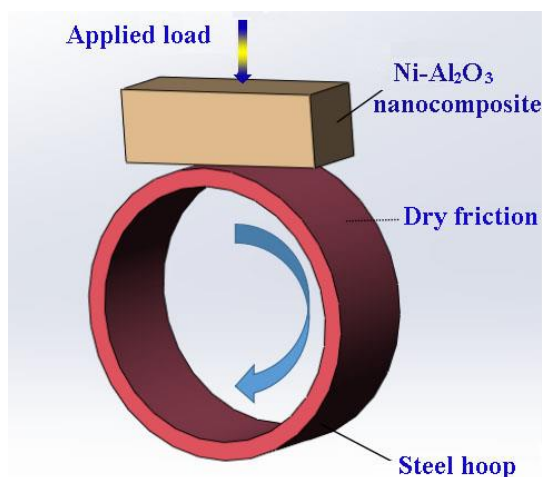


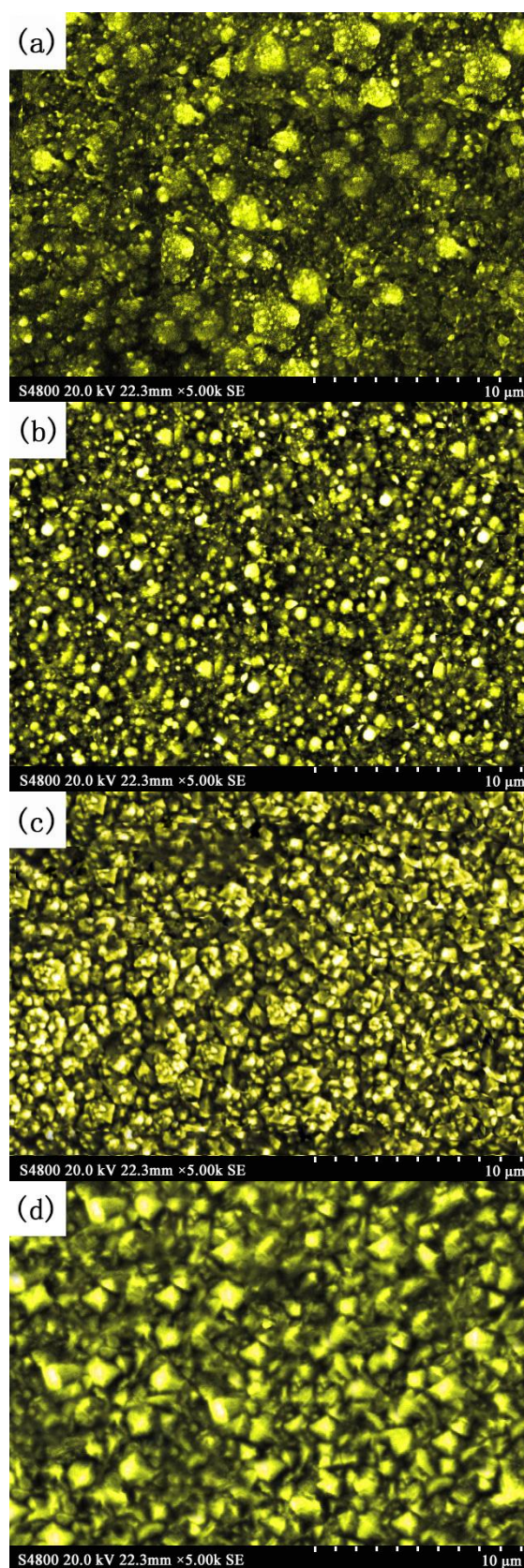
**Figure 2.** Diagram showing experimental setup for the wear resistance tests.

Corrosion experiments were performed using a three-electrode configuration by utilizing CS350 electrochemical workstation with 4 wt% NaCl solution as the electrolyte. Saturated calomel electrode (SCE) and Pt acted as reference and counter electrodes, respectively. Electrochemical impedance spectroscopy (EIS) was performed in the  $10^2\sim 10^5$  Hz range at an open-circuit voltage equal to 10 mV.

### 3. RESULTS AND DISCUSSION

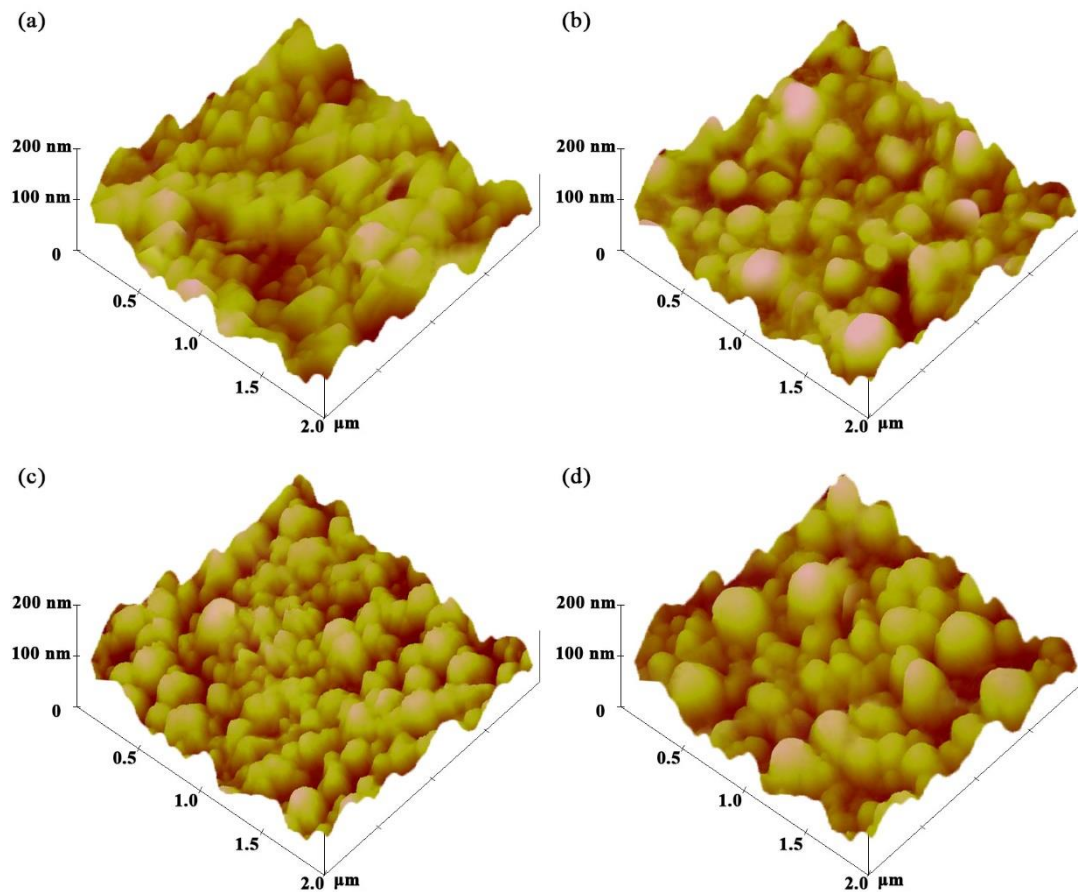
#### 3.1 Surface morphology

SEM analysis of Ni-SiC NCs fabricated at 100, 200, 300, and 400 W showed that ultrasonic power significantly affected NC morphologies (see Fig. 3). Samples Ni-SiC-100 and Ni-SiC-200, fabricated at ultrasonic power equal to 100 and 200 W, respectively, had loose and somewhat coarse microstructure with large grains (see Fig. 3a-b). Ni-SiC-300 NC, deposited at 300 W, showed smooth and fine-grained surface morphology with SiC NPs evenly distributed on the NC surface (see Fig. 3c). Ni-SiC-400 sample, obtained at 400 W, contained smaller amount of SiC NPs and also demonstrated coarse and loose microstructure (see Fig. 3d). The results are in agreement with those reported by A. Bahgat Radwan [22].



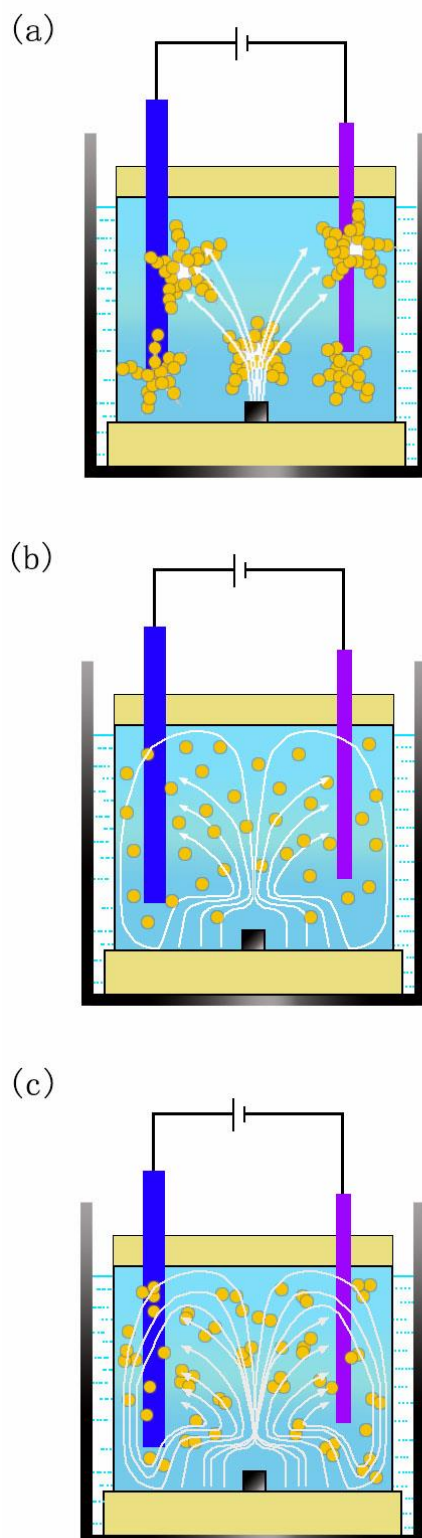
**Figure 3.** SEM micrographs Ni-SiC NCs fabricated at ultrasonic power equal to (a) 100 W, (b) 200 W, (c) 300 W, and (d) 400 W.

Fig. 4 displays the AFM morphologies of Ni-SiC NCs synthesized at different ultrasonic powers. AFM analysis confirmed SEM observations that Ni-SiC-100 and Ni-SiC-200 samples contained grains larger than those in the Ni-SiC-300 and Ni-SiC-400 samples (see Fig. 4a-d). AFM also confirmed compact and smooth surface texture as well as homogeneously dispersed SiC NPs on the NC surface obtained at 300 W (Ni-SiC-300 sample, see Fig. 4c). A.F. Zimmerman *et al.* [23] found that suitable plating parameters could cause the SiC nanoparticles evenly distributed in Ni-SiC NCs.



**Figure 4.** AFM results for Ni-SiC NCs synthesized at ultrasonic power equal to (a) 100 W, (b) 200 W, (c) 300 W, and (d) 400 W.

Mechanism explaining why ultrasonic power affected particle morphology and SiC NP dispersion in the Ni matrix is schematically shown in Fig. 5. At 100 and 200 W, SiC NPs agglomerated and remained suspended in the plating solution (see Fig. 5a). These SiC agglomerates were larger than a nanometer in size. Such large SiC NPs present in the Ni-SiC-100 and Ni-SiC-200 samples could not impede Ni grain growth sufficiently, which resulted in the formation of coarse Ni crystals and loose microstructures. At 300 W, SiC NPs were well-dispersed and suspended in the solution and did not agglomerate, maintaining their nanometer sizes. This allowed numerous SiC NPs to be homogeneously incorporated in the Ni-matrix and to generate a large number of nucleation sites inside expanding and growing Ni-matrix.



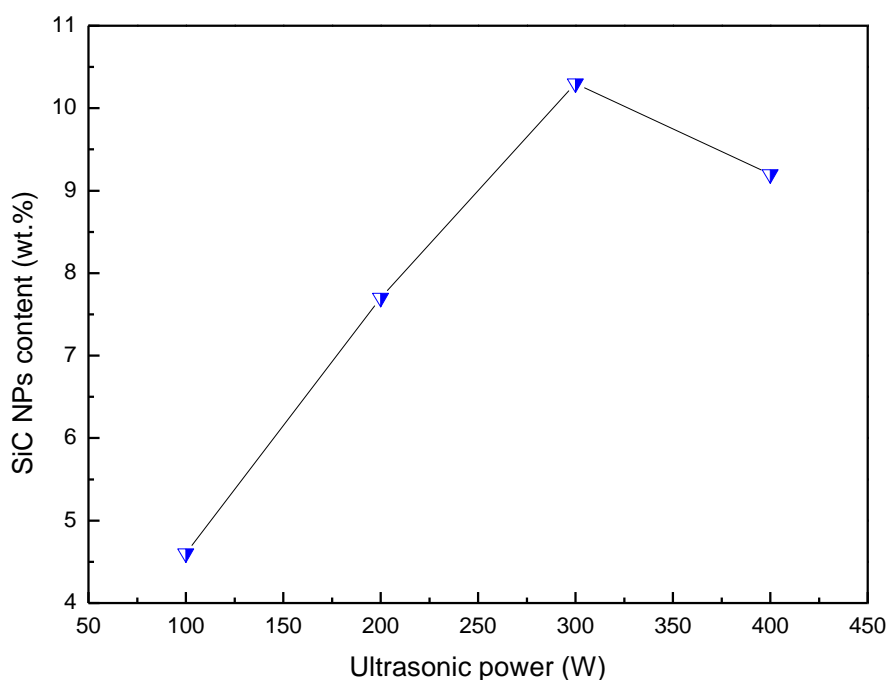
**Figure 5.** Schematic showing mechanism of ultrasonic dispersion of SiC NPs in the plating solution.

A large number of nucleation sites helped to impede Ni grain growth [24] and to obtain a fine-grained and smooth surface (see Fig. 5b). At 400 W, excessive ultrasonic power prevented simultaneous deposition of SiC NPs and Ni<sup>2+</sup> at the cathode. As a result, weakly-bonded SiC NPs were

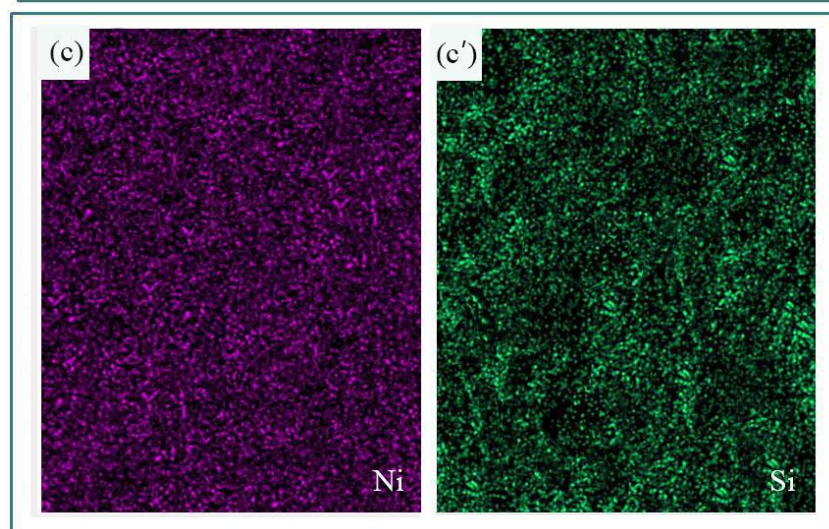
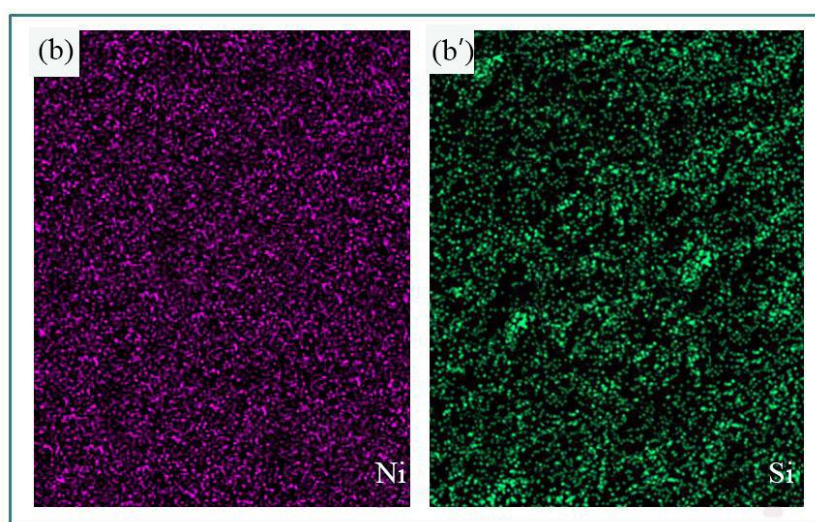
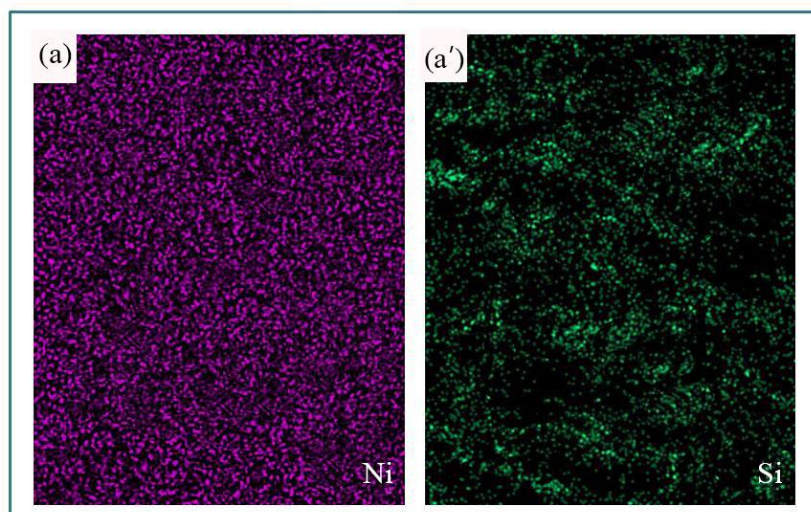
flushed back into the plating solution. Thus, an insufficient amount of SiC NPs became deposited on the Ni matrix of the Ni-SiC-400 sample, which, in turn, resulted in fast Ni grain growth and overall coarse and loose microstructure of the whole NC (see Fig. 5c).

### 3.2 Chemical composition and element distribution of the Ni-SiC NCs

Figs. 6 and 7 present the chemical composition and element distribution of the Ni-SiC NCs deposited at ultrasonic powers of 100, 200, 300 and 400 W, respectively. As ultrasonic power during NC synthesis increased, SiC NP content first fleetly increased and then slightly reduced (see Fig. 6). At 100 W, SiC NP content in the Ni-SiC-100 NC was 4.6 wt.%. However, at 300 W, SiC NP content in the Ni-SiC-300 sample was 10.3 wt.%, which is the highest SiC content achieved out of all other samples prepared in this work. At low ultrasonic power, SiC NP agglomerated, and their deposition at the cathode slowed down, which decreased their content in the Ni-SiC NC. Excessive ultrasonic power (such as 400 W) not only constrained the co-deposition of SiC NP and  $\text{Ni}^{2+}$  on the cathode but also detached weakly adsorbed SiC NP from the cathode surface, which resulted in low SiC NP content in the NC [25]. These processes also decreased the number of the nucleation sites in the Ni matrix, which was favorable for the growth of large Ni grains. Element distribution analysis showed the presence of both Ni and SiC on the surfaces of all NCs (see Fig. 7). However, only the NC obtained at 300 W (Ni-SiC-300 sample) contained the highest SiC amount and its most uniform distribution.



**Figure 6.** Influence of ultrasonic power on the SiC contents of Ni-SiC NCs.



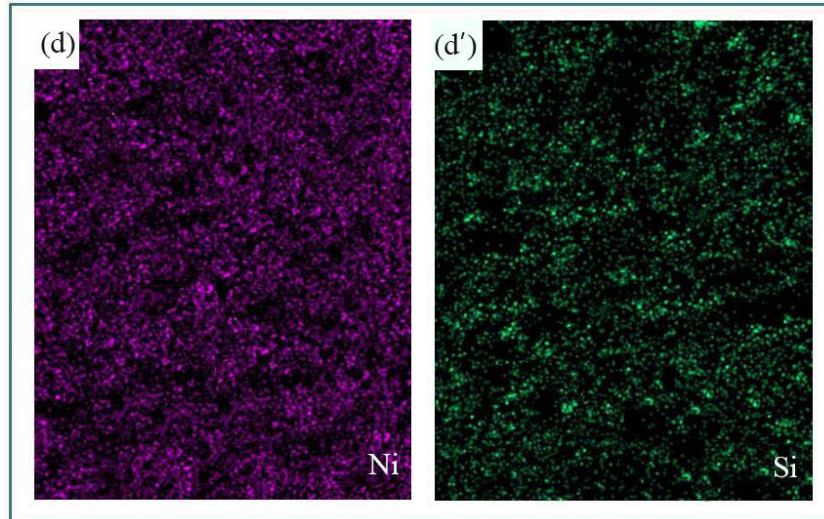


**Figure 7.** Element distribution for Ni-SiC NC fabricated at ultrasonic power equal to (a) 100 W, (b) 200 W, (c) 300 W, and (d) 400 W. Purple and blue colors correspond to Ni and Al, respectively.

### 3.3 Phase compositions of the Ni-SiC NCs

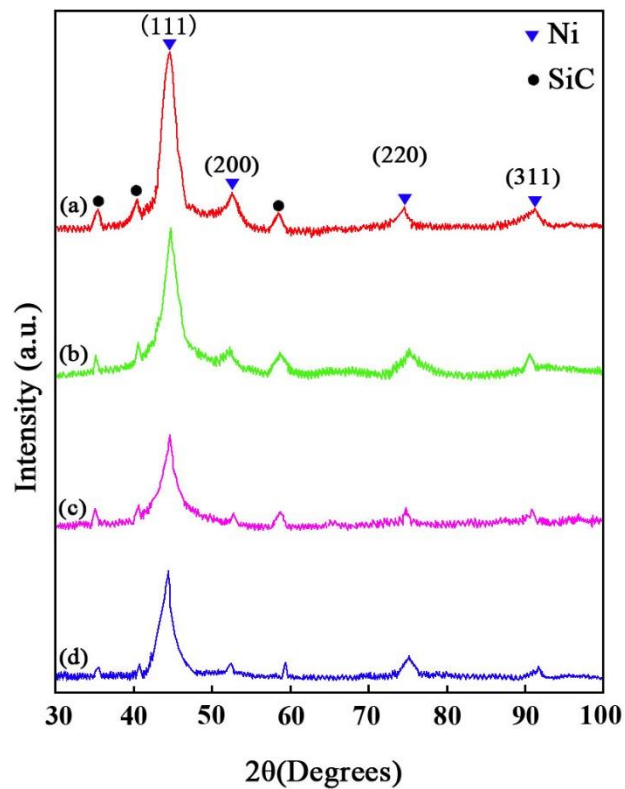


**Figure 8.** XRD patterns of Ni-SiC NCs fabricated at ultrasonic power equal to (a) 100 W, (b) 200 W, (c) 300 W, and (d) 400 W.

XRD spectra of all Ni-SiC NCs produced in this work demonstrated strong peaks belonging to

(1 1 1), (2 0 0), (2 2 0) and (3 1 1) planes of metallic Ni and weak peaks corresponding to SiC, which confirms presence of SiC NP in the Ni matrix (see Fig. 8). For Ni grains, the strong diffractions peaked were noticed at  $44.8^\circ$ ,  $52.2^\circ$ ,  $76.7^\circ$  and  $92.4^\circ$ , respectively. For SiC NPs, three weak diffractions located at  $34.2^\circ$ ,  $41.5^\circ$  and  $59.8^\circ$  were observed and assigned to (1 1 1), (2 0 0) and (2 2 0) planes, respectively. In addition, XRD peaks corresponding to Ni matrix first broadened but then narrowed as ultrasonic power was raised from 100 W to 400 W. This further testifies that the crystalline size of Ni-SiC NC could be controlled by applying appropriate ultrasonic power (which was 300 W in this work).

### 3.4 Mechanical properties of Ni-SiC NCs

Microhardness values obtained for Ni-SiC NCs obtained in this work first increased and then decreased as power during NC fabrication increased (see Fig. 9). The highest microhardness value (equal to 906.7 Hv) was obtained for the NC obtained at 300 W (Ni-SiC-300 sample) because this sample possessed the smallest grain sizes and the highest content of the reinforcing filler (SiC NPs). These results correlate with the Hall-Petch equation on the reverse correlation between microhardness and the matrix grain sizes [26].

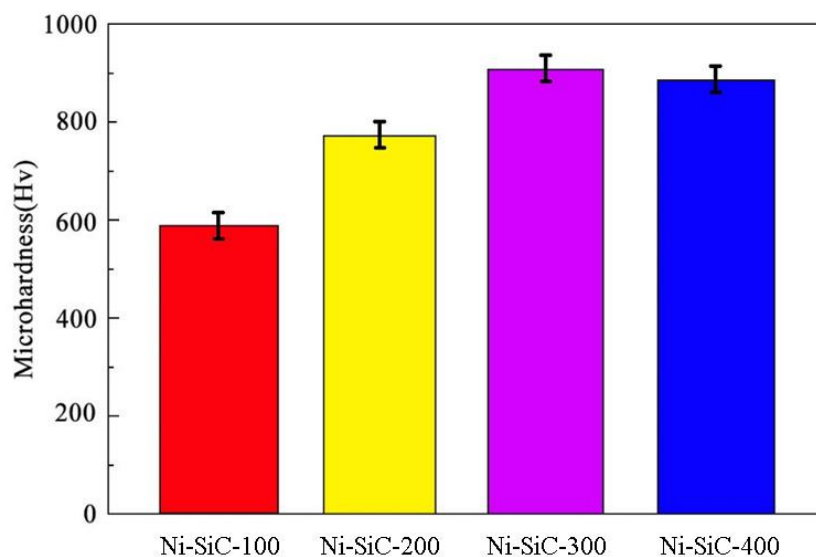


**Figure 9.** Microhardness test results obtained for Ni-SiC NCs fabricated at ultrasonic powers equal to 100, 200, 300 and 400 W.

### 3.5 Wear experiments

#### 3.5.1 Wear rate

Influence of ultrasonic power used to synthesize Ni-SiC NCs on their wear rate is shown in Fig. 10. Wear rates of all NCs increased very rapidly as wear distance raised from 0 to 30 m because the

counterpart of the steel hoop polished and flattened the sample surface during the initial stage. When the wear distance increased from 30 to 150 m, the NC wear rate change slowed down. The wear rate of the Ni-SiC-300 sample (which is equal to 17.8 mg/min) was the lowest out of all composites synthesized in this work. Thus, Ni-SiC-300 samples obtained at 300 W ultrasonic power had the best wear resistance. Ni-SiC-100 NCs demonstrated a maximum average wear rate equal to 37.5 mg/min. According to the Archard's equation [27], wear rates of composites based on metal matrices decrease as composite microhardness values increase. This agrees with our results very well: Ni-SiC-300 NC showed the highest microhardness and the lowest wear rate.

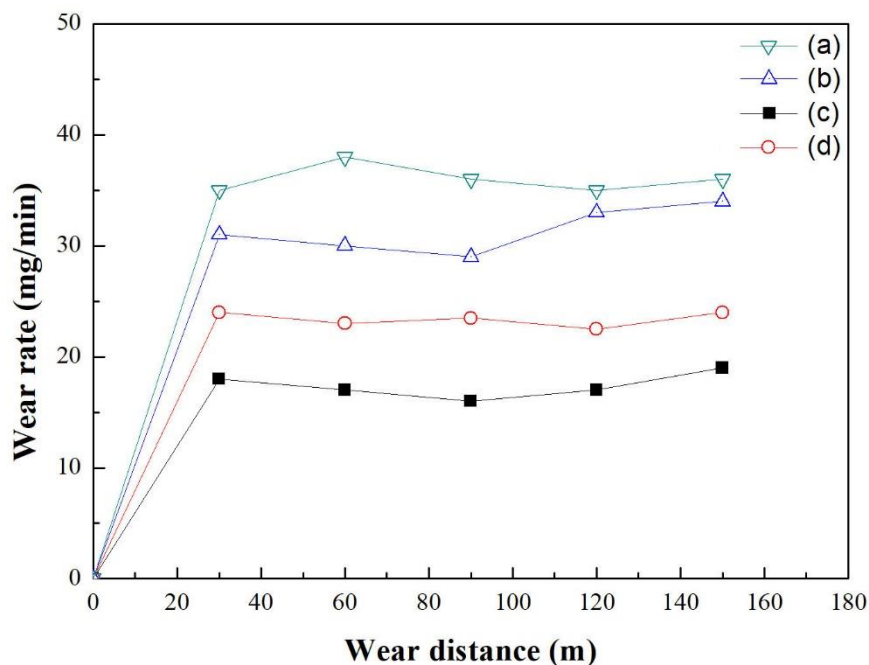


**Figure 10.** Wear rate of the Ni-SiC NCs synthesized at ultrasonic power equal to (a) 100 W, (b) 200 W, (c) 300 W, and (d) 400 W.

### 3.5.2 Morphologies of the surfaces after wear tests

SEM and LSCM results for the surfaces of the Ni-SiC NCs synthesized at 100 and 300 W after they were subjected to the wear tests are shown in Fig. 11. Ni-SiC-100 sample showed wider and deeper wear tracks than Ni-SiC-300 NC, which indicates poorer wear resistance of Ni-SiC-100 NC. Typically, the wear track width of a composite is inversely proportional to its microhardness [28].

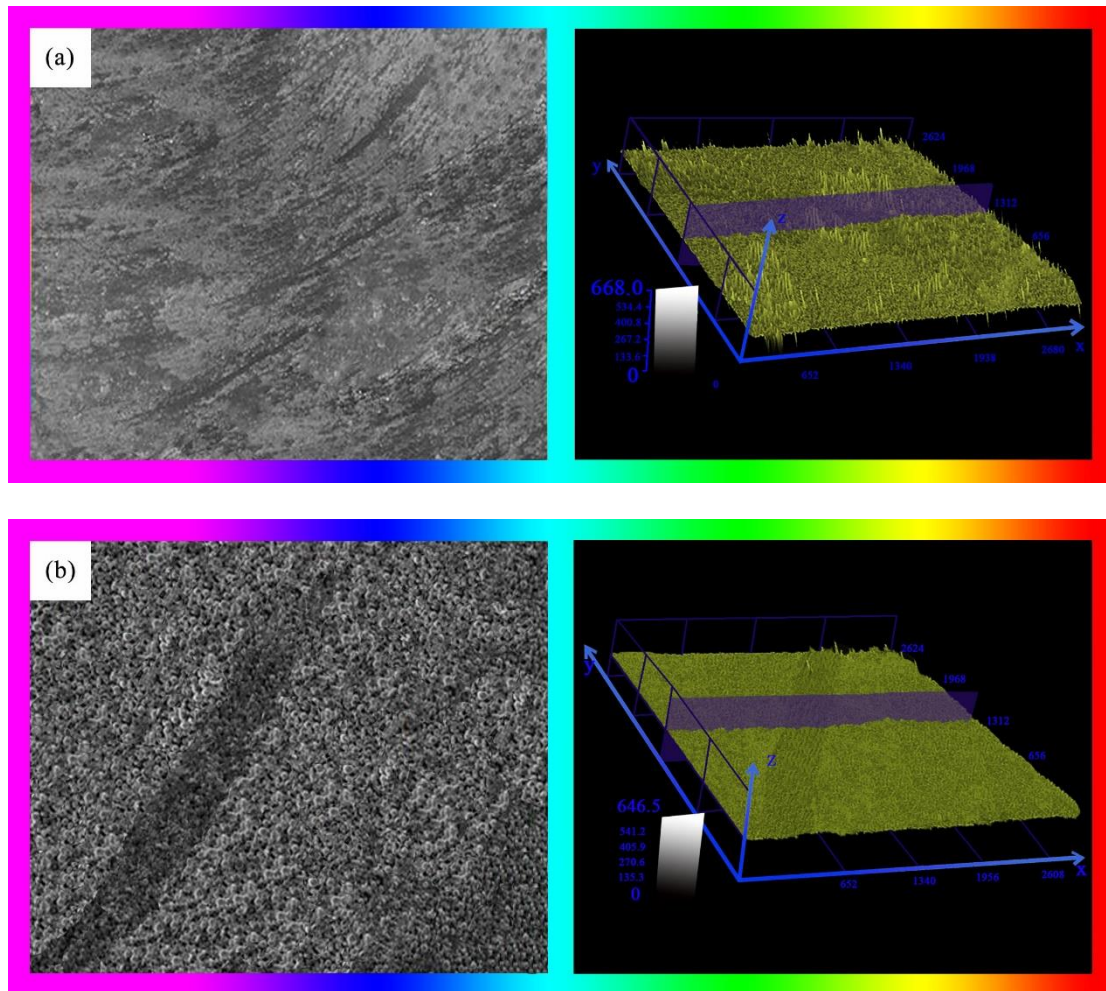


**Figure 11.** SEM and LSCM analysis results obtained for surfaces of Ni-SiC NCs obtained at (a) 100 W and (b) 300 W ultrasonic power after wear tests.

Because microhardness of the Ni-SiC-300 NC was higher, wear tracks were narrower and shallower than those for other samples obtained in this work. Thus, these results again corroborate superior wear resistance of the NC obtained at ultrasonic power equal to 300 W.

### 3.5.3 Friction coefficients

Friction coefficients of all Ni-SiC NCs obtained in this work are shown in Fig. 12. Ni-SiC-300 sample displayed the smallest friction coefficient equal to 0.33, while Ni-SiC-100 NC had the highest (equal to 0.82). SiC content and NC microhardness were the main factors determining Ni-SiC NC friction coefficients [29]. At higher filler contents (such as in Ni-SiC-300 sample), SiC NPs detached from the matrix forming rolling grains, which changed the friction mode between the NC and the steel hoop from sliding to rolling. As a result, the friction coefficient decreased.

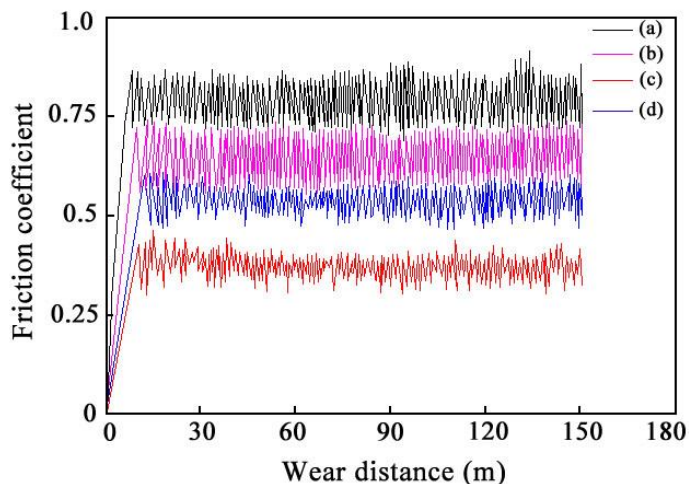


**Figure 12.** Friction coefficients of Ni-SiC NCs fabricated at ultrasonic power equal to (a) 100 W, (b) 200 W, (c) 300 W, and (d) 400 W.

### 3.6 Corrosion analysis

Tafel curves of all Ni-SiC NCs obtained in this work are shown in Fig. 13. Corresponding corrosion potential ( $E_{corr}$ ) and current density ( $i_{corr}$ ) are presented in Table 2.

**Table 2.** Corrosion data obtained from the electrochemical tests of the Ni-SiC NCs.

Nanocomposite	$E_{corr}$ (V)	$i_{corr}$ ( $\mu\text{A}/\text{mm}^2$ )
Ni-SiC-100	-0.438	0.076
Ni-SiC-200	-0.432	0.049
Ni-SiC-300	-0.311	0.032
Ni-SiC-400	-0.379	0.043

Ni-SiC-100 Nc showed the highest  $i_{corr}$  equal to  $0.076 \mu\text{A}/\text{mm}^2$ , which illustrates the poorest corrosion resistance, while the Ni-SiC-300 NC demonstrated the lowest  $i_{corr}$  value (equal to  $0.032 \mu\text{A}/\text{mm}^2$ ). Thus, the Ni-SiC-300 sample had the best corrosion resistance very likely because of the high SiC NP content.

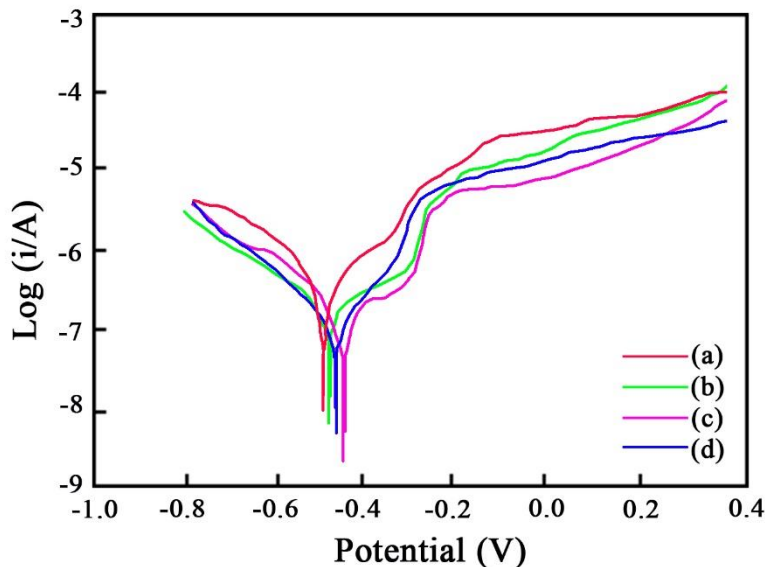


**Figure 13.** Potentiodynamic polarization curves for the Ni-SiC NCs synthesized at ultrasonic power equal to (a) 100 W, (b) 200 W, (c) 300 W, and (d) 400 W.

Nyquist plots of Ni-SiC NCs obtained at different ultrasonic powers are shown in Fig. 14 and Table 3, respectively. The lowest impedance was observed for the Ni-SiC-100 NC, which confirms our earlier conclusions about its worst anticorrosion ability. Ni-SiC-300 NC showed the highest impedance, which is indicative of the best corrosion resistance of this sample comparing to all others synthesized in this work. Thus, an appropriate ultrasonic power during NC synthesis not only promoted the formation of the smooth and fine-grained surfaces but also resulted in the best ability of the composite to withstand corrosive penetration of the etchant solution. The phenomenon is consistent with the study reported by X. Xu *et al.* [30].

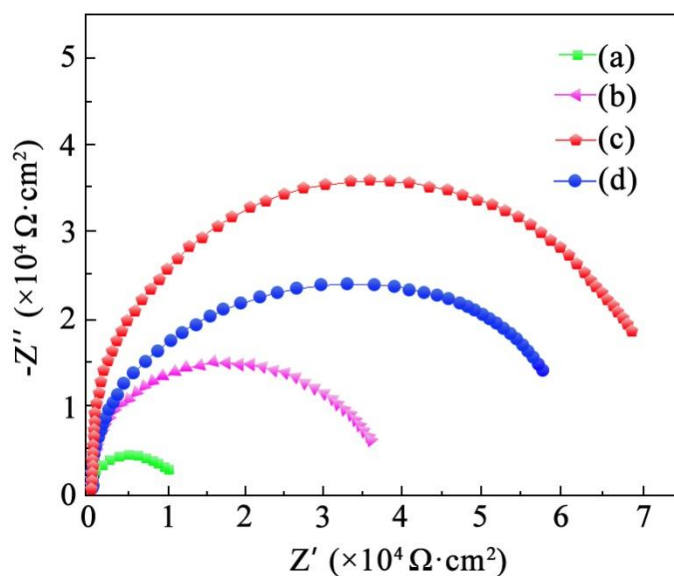


**Figure 14.** Nyquist plots for the Ni-SiC NCs synthesized at ultrasonic power equal to (a) 100 W, (b) 200 W, (c) 300 W, and (d) 400 W.

**Table 3.** Corrosion parameters of Ni–SiC NCs deposited at various ultrasonic powers.

Ultrasonic power (W)	$R_s$ ( $\Omega \cdot \text{cm}^2$ )	$R_{ct}$ ( $\Omega \cdot \text{cm}^2$ )	$C_{dl}$ ( $\mu\text{F}/\text{cm}^2$ )
100	3.75	5126	51.24
200	4.82	9451	42.71
300	8.19	25318	25.16
400	7.04	16274	29.98

#### 4. CONCLUSION

(1) Samples Ni-SiC-100 and Ni-SiC-200, fabricated at ultrasonic power equal to 100 and 200 W, respectively, had loose and somewhat coarse microstructure with large grains. Ni-SiC-300 NC, deposited at 300 W, showed smooth and fine-grained surface morphology with SiC NPs evenly distributed on the NC surface. At 100 W, SiC NP content in the Ni-SiC-100 NC was 4.6 wt.%. However, at 300 W, SiC NP content in the Ni-SiC-300 sample was 10.3 wt.%, which is the highest SiC content achieved out of all other samples prepared in this work.

(2) XRD peaks corresponding to Ni matrix first broadened but then narrowed as ultrasonic power was raised from 100 W to 400 W. This further indicates that the crystalline size of Ni-SiC NC could be controlled by applying appropriate ultrasonic power. In addition, the highest microhardness value (equal to 906.7 Hv) was obtained for the NC obtained at 300 W (Ni-SiC-300 sample) because this sample possessed the smallest grain sizes and the highest content of the reinforcing filler (SiC NPs).

(3) When the wear distance raised from 30 to 150 m, the NC wear rate change slowed down. The wear rate of the Ni-SiC-300 sample (which as equal to 17.8 mg/min) was the lowest out of all composites synthesized in this work. Besides, Ni-SiC-100 sample showed wider and deeper wear tracks than Ni-SiC-300 NC, which indicates poorer wear resistance of Ni-SiC-100 NC.

(4) Ni-SiC-100 Nc showed the highest  $i_{corr}$  equal to  $0.076 \mu\text{A}/\text{mm}^2$ , which illustrates the poorest corrosion resistance, while the Ni-SiC-300 NC demonstrated the lowest  $i_{corr}$  value (equal to  $0.032 \mu\text{A}/\text{mm}^2$ ). Ni-SiC-300 NC showed the highest impedance, which is indicative of the best corrosion resistance of this sample comparing to all others synthesized in this work.

#### ACKNOWLEDGEMENT

This work has been supported by the National Natural Science Foundation of China (Grant Nos. 51974089, 51674090), and Natural Science Foundation of Heilongjiang Province of China (Grant No. LC2018020).

#### References

1. M. Sajjadnejad, H. Omidvar, and M. Javanbakht, *Surf. Eng.*, 33 (2017) 94.
2. C. Ma, M. Jiang, and F. Xia, *Surf. Rev. Lett.*, 24 (2016) 17500631.
3. F. Xia, W. Jia, M. Jiang, and J. Wang, *Ceram. Int.*, 43 (2017) 14623.
4. H. Zhou, W. Wang, Y. Gu, X. Fang, and Y. Bai, *Strength Mater.*, 1 (2017) 1.
5. M. Sajjadnejad, H. Omidvar, M. Javanbakht, and A. Mozafari, *J. Alloy. Compd.*, 704 (2017) 809.

6. W. Jiang, L. Shen, M. Qiu, X. Wang, M. Fan, and Z. Tian, *J. Alloy. Compd.*, 762 (2018) 115-124.
7. C. Ma, W. Yu, M. Jiang, and F. Xia, *Ceram. Int.*, 44 (2018) 5163.
8. F. Xia, Q. Li, C. Ma, and X. Guo, *Ceram. Int.*, 46(2020) 2500.
9. M. Alizadeh, and A. Cheshmpish, *Appl. Surf. Sci.*, 466 (2019) 433.
10. F. Xia, C. Liu, F. Wang, M. Wu, J. Wang, H. Fu, and J. Wang, *J. Alloy. Compd.*, 490 (2010) 431.
11. B. Li, W. Zhang, W. Zhang, and Y. Huan, *J. Alloy. Compd.*, 702 (2017) 38.
12. Q. Fan, Y. Gao, Y. Zhao, Q. Yang, L. Guo, and L. Jiang, *Mater. Lett.*, 215 (2018) 242.
13. A. Aal, M. Bahgat, and M. Radwan, *Surf. Coat. Tech.*, 201 (2006) 2910.
14. F. Xia, W. Jia, C. Ma, R. Yang, Y. Wang, and M. Potts, *Appl. Surf. Sci.*, 434 (2018) 228.
15. A. Mukhtar, M. Tan, H. Hu, L. Liu, T. Mehmood, and B. Khan, *J. Nanosci. Nanotechno.*, 18 (2018) 1296.
16. M. Shourgeshty, M. Aliofkhazraei, and A. Karimzadeh, *Surf. Eng.*, 1 (2018) 1.
17. M. Alizadeh and A. Cheshmpish, *Appl. Surf. Sci.*, 466 (2019) 433.
18. S. Dehgahi, R. Amini, and M. Alizadeh, *J. Alloys Compd.* 692 (2017) 622.
19. F. Xia, M. Wu, F. Wang, Z. Jia, and A. Wang, *Curr. Appl. Phys.*, 9 (2009) 44.
20. R. Sen, S. Das, and K. Das, *J. Nanosci. Nanotechno.*, 10 (2010) 8217.
21. E. Beltowska-Lehman, P. Indyka, A. Bigos, M. Szczerba, and M. Kot, *Mater. Des.*, 80 (2015) 1.
22. A. Bahgat Radwan, and R.A. Shakoor, *Ceram. Int.*, 46 (2020) 5556.
23. A.F. Zimmerman, D.G. Clark, K.T. Aust, and U. Erb, *Mater. Lett.* 52 (2002) 85
24. X. Chen, J. Peng, X. Li, F. Deng, J. Wang, and W. Li, *J. Mater. Sci. Lett.*, 20 (2001) 20570.
25. F. Xia, J. Jiao, J. Ding, L. Miao, *Ordnance mater. Sci, Eng.*, 35 (2012) 45 (in Chinese).
26. H. Gül, F. Kılıç, S. Aslan, A. Alp, and H. Akbulut, *Wear*, 267 (2009) 976.
27. K. Hou, H. Sheu, and M. Ger, *Appl. Surf. Sci.*, 308 (2014) 372.
28. C. Sun, X. Liu, C. Zhou, C. Wang, and H. Cao, *Ceram. Int.*, 45 (2019) 1348.
29. R. Mousavi, M. Bahroloom, and F. Deflorian, *Mater. Des.*, 110 (2016) 456.
30. X. Xu , J. Miao, Z. Bai, Y. Feng, Q. Ma, W. Zhao, *Appl. Surf. Sci.*, 258 (2012) 8802.